Himalayan Journal of Science and Technology, Vol. (2021) 2-7

Himalayan Journal of Science and Technology

Original Article

doi: https://doi.org/10.3126/hijost.v5i01.42079

Dust Structure nearby G229-03

[a]Hem Shrestha, [b]Ajay Kumar Jha, [c]Saroj Nepal, [d]Aatmaram Tiwari, [e]Kamana Bantawa, [f]Dhiren Subba Limbu*

[a]Department of Physics, Central Campus of Technology, Tribhuvan University, Dharan
[b]Central Department of Physics, Tribhuvan University, Kathmandu
[c]Department of Physics, Mechi Multiple Campus, Bhadrapur
[d]Department of Physics, Mahendra Morang Adarsha Multiple Campus, Biratnagar
[e]Department of Microbiology, Mahendra Morang Adarsha Multiple Campus, Biratnagar
[f]Department of Microbiology, Central Campus of Technology, Dharan

*Corresponding email: hem.shrestha@cct.tu.edu.np

Abstract

The Sky View Virtual Observatory was used for the systematic search of dust structures within the far-infrared loop G229-03. The source (object) responsible for the formation of the cavity of interest was detected by the Set of Identifications, Measurements, and Bibliography for Astronomical Data (SIMBAD) database. The total mass of the loop was 8.50031×10^{29} kg which is about 0.425 times the mass of the Sun at a distance of 1300 pc. The size of the cavity was 3.67° × 3.6°, whereas its core size was 0.531° × 0.255° located at R.A. (J2000) = $7^h10^m0.8^s$ and Dec.(J2000) =$15^h55^m30^s$. The minimum and maximum temperatures were between 20.24 ± 1.16 K and 18.63 ± 1.96 K respectively. In the core region, the average temperature was 19.53 K, approximately equal to Gaussian center 19.267 K with an offset temperature of 0.4 K showing that the core region of the cavity is dynamically stable. The Far-infrared loop was found to be located within a 1° radius around the high-velocity cloud HVC oriented by 45° to the plane of the sky. The inclination angle of the core of the loop was greater than 60° whereas the inclination angle for the larger structure was 13.71°. The Gaussian distribution of temperature was well fitted with the center of 19.267 K which shows that the cavity was in thermal equilibrium and the outer region with offset temperature of about 35 K suggesting that the loop was dynamically unstable possibly due to high-velocity cloud.

Article Info

Article history:

Received date: 27 September 2021
Accepted date: 23 December 2021

Keywords:
Interstellar Medium
Interstellar Dust
Flux Density
Inclination Angle
Cavity Structure

1. Introduction

The content of interstellar medium (ISM) is matter and field which further contains gas and dust so that there exist different structures such that jets, shells, nebula, filaments, arc, loops, and cavities. The high-pressure events create bubbles and superbubbles which are assumed to be responsible for the formation of cavities (Jha & Aryal, 2018). The development of nonlinear instabilities in the ISM may form large cavities as well, without stellar energy injection (Wada et al., 2000). Due to the different interaction processes in the interstellar medium Far infrared (FIR) dust structures are formed (Weinberger & Armsdorfer, 2004). On 100 and 60 μm, Infrared Astronomical Satellite IRAS maps Aryal et al. (2010) found two bipolar dust emission structures centered on NGC 1514. Aryal et al. (2009) observed that the planetary nebulae NGC 2899 are located at the center of a large (14 pc × 11 pc) quadrupolar cavity (Aryal et al., 2009). The (IRAS) consists of a cryogenically cooled telescope orbiting above the Earth's atmosphere to make an unbiased all-sky survey at 12, 25, 60, 100 μm IRAS surveyed the entire sky at several wavelengths (Schulz & Consortium, 2010). The 60 μm and 100 μm images can proceed in ALADIN software, from which we can calculate physical properties like mass, temperature, flux density variation (Gautam & Aryal, 2019). Jha et al., 2017 studied the dust color temperature at 60 μm and 100 μm of four infrared loops namely G007+18, G147+07, G214-01, and G323-02 which were found to be located around Pulsars PSR J1720-1633, PSR J0406+6138, PSR J06520142, and PSR J1535-5848

respectively (Jha et al., 2017). The photographs of the Milky Way galaxy referred to such large-scaled loop-shaped dust and gas structures as "Cosmic Bubble Bath" were examined by Brand and Zealey, in 1957 (Brand & Zealey, 1975). Similarly, 145 loops were distinguished and their energetics and organizations were studied using 100 μm and 60 μm IRAS maps by Kiss et al., 2004 (Kiss et al., 2004). Likewise, Koenyves et al., 2007 identified 462 loops, analyzed their individual FIR properties and their distribution in ISM, and concluded that the formation of these structures is presided by supernovae and stellar winds (Köenyves et al., 2007).

The use of SIMBAD ((http://simbad.u-strasbg.fr/simbad/sim-fcoo) database and cross-checked from Sky View Virtual Observatory ((http://skyview.gsfc.nasa.gov/current/cgi/query.pl) respectively, using data reduction software ALADIN 2.5 and other software Origin 5.0 and 8.0, etc. had made this research easy. Hence, the physical properties of the core region of the selected loop were investigated during a systematic search on IRAS maps located close to the (HVC) 0070.6+15.3-128 from which it will be easier to find its effect for the formation of a cavity in ISM. The dust color temperature of the core region was compared with its outer edge and the distribution of dust color temperature and dust mass were calculated. Additionally, the inclination angle was calculated to know about the morphological structure and the orientation of the cavity in the plane of the sky.

2. Materials and Method

The following method was used to find the size, dust color temperature, dust mass, and inclination angle.

2.1 Dust Color Temperature Estimation:

The dust color temperature of all pixels of selected Far Infrared loop candidates was estimated. In addition, the data from the GIRL catalog was used to calculate the average dust color temperature of all Far infrared loops. For the calculation of dust color temperature, the method proposed by Köenyves et al. (2007) and Dupac et al. (2003) was used. The corrected flux density at each pixel inside the region of interest was calculated from a 100 μm image. Similarly corrected flux densities were calculated from the IRAS 60 μm image (Dupac et al., 2003). Using the ratio of flux densities in IRAS 60 μm to the flux density in 100 μm, dust color temperature was calculated as,

$$\mathrm{Td} = \frac{-96}{\ln\{R \times (0.6)^{(3+\beta)}\}} \qquad (1)$$

Where R is given by,

$$\mathrm{R} = \frac{F\,(60\mu m)}{F\,(100\mu m)}$$

Where F (60μm) and F (100μm) are the flux densities at 100 μm and 60 μm. The value of β depends upon the dust properties like composition, size of dust, and compactness. For example, a pure black body would have β=0, the amorphous layer lattice matter has β~1 and the metals and crystalline dielectrics have β~2 (Dupac et al., 2003).

2.2 Dust Mass Estimation

The dust mass of a cloud at a known distance can be calculated with the help of the measurement based on the flux density, temperature, emissivity, and the size of grains (Hildebrand, 1983). For the calculation of dust mass, an idealized cloud composed of spherical grains of uniform size, composition, and the temperature was considered. The distance to the region of interest was also used in the calculation of dust mass. The distance is recommended to be 1300 pc and we use this distance to calculate dust mass in our calculation. The resulting dust mass depends upon the properties of a dust grain, dust temperature, and the distance to the object. The dust masses were estimated using a formula by Hildebrand (Hildebrand, 1983).

$$\mathrm{Mdust} = \frac{4a\rho}{3Q_\nu}\left[\frac{S_\nu D^2}{B(\nu,T)}\right] \qquad (2)$$

This expression for dust mass may be applicable only for clouds with uniform spherical grains and that the radius, must be known for the grains in each cloud under consideration.

Where,

a = Weighted grain size

ρ = Grain density

Qν = Grain emissivity

Sν = Flux density

D = Distance for the structure

B(ν, T) = Plank's function, which is the function of

temperature and frequency and is given by the expression.

$$B(\nu,T)=\frac{2h\nu^3}{c^2}\left[\frac{1}{\exp\left(\frac{h\nu}{kT}\right)-1}\right] \qquad (3)$$

Where,

h = Planck's constant

c = Speed of light

ν = Frequency at which the emission is observed

T = The average temperature of the region (Hildebrand, 1983).

The value of various parameters we used in calculation dust mass in our region of interest are as follows:

a = 0.1μm (Young et al., 1993)

ρ = 3000 kg/m3 (Young et al., 1993)

Qν = 0.010 for 100 μm and 0.0046 for 60 μm

respectively (Young et al., 1993)

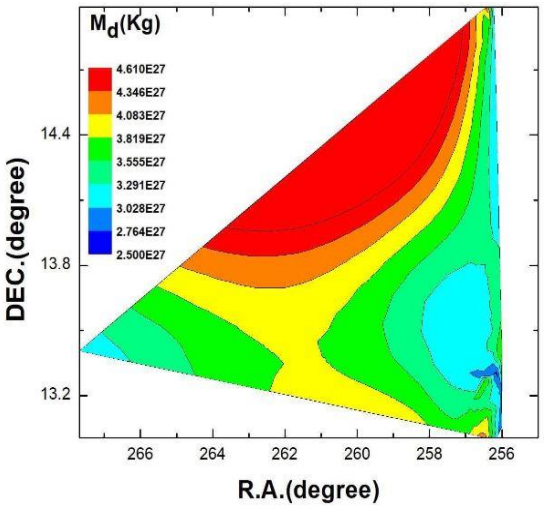

Figure 1: Three-dimensional contour plot of dust mass

2.3 Inclination Angle

The inclination angle is the angle between the line of sight and normal to the plane of the Sky. The inclination angle (i) of the structure can be determined by the equation below

$$\cos 2i = \frac{\left(\frac{b}{a}\right)^2 - q^2}{1-q^2} \qquad (4)$$

Where b/a is the axial ratio and q is the intrinsic flatness. Hlomberg used the value of q to be 0.33 for oblate spheroid. This formula was used for the calculation of the inclination angle of the core and whole loop (Hlomberg, 1946).

3. Results and Discussion

In this study, physical properties of a loop-like structure G229-03 were done in which galactic latitude was found in the far-infrared IRAS maps. The size of the Far-infrared loop G229-03 was found to be 3:7° × 3:6° (Koenyves et al., 2007) having core size 0:531° × 0:255° located at R.A.(J2000) = 7h10m0.8s and Dec.(J2000) = 15h55m30s (Figure-1). Therefore the core region of the loop was only about 1.025 % of the whole loop. There were altogether 343 pixels in the selected cavity. The maximum portion of the cavity was filled with the pixels of mass 4 × 1027 kg which is shown by red color in figure. The minimum mass of the range 2 × 1027 kg is shown by dark and faint blue color in figure 1. The portion with the minimum mass was distributed randomly throughout the cavity and it may be due to blowing or shock waves created by various stellar or wind blowing objects like pulsars, infrared sources, radio sources, Asymptotic Giant Branch (AGB), and high-velocity clouds. In the case of cavity G229-03, HVC named 0070.6 + 15.3-12.8 was at a distance of 2449.3 arcs second from the cavity. The random distribution of lower mass may be due to the HVC (Figure 1).

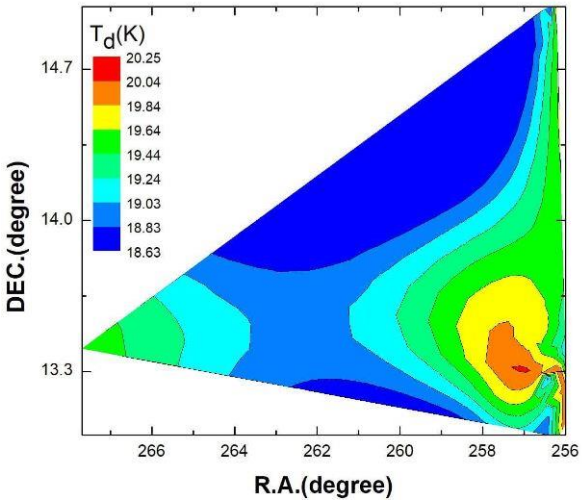

Figure 2: Three-dimensional contour plot of dust color temperature

The total mass of the loop was found to be 8.50031 × 1029 kg about 0.425 times the mass of Sun at a distance of 1300 pc. In a similar study carried out by Jha and Aryal (2017), the total mass of the loop was found to be 2.55 × 1027 kg. The reason behind the higher value of the total mass of dust structure in this study may be due to the difference in nearby

objects around dust structure (Jha et al., 2017). A three-dimensional contour plot of temperature is shown in Figure 2.

The regions with a maximum temperature of the range 20.25 K are very small and lie in the southeast part of the figure which is shown by red and faint orange color. Most of the middle parts of the cavity of interest were filled with the minimum temperature of the range of 18.5 K which is shown by dark blue and faint blue colors. Mass was large in our cavity where the temperature was minimum. The dust mass contour plot seems to follow an expected trend that is the higher density at a lower temperature which is in good agreement with the results found by Jha and Aryal in 2017 (Jha et al., 2017).

The distribution of dust mass is represented by Gaussian fit which is indicated by the solid curve in Figure 3.

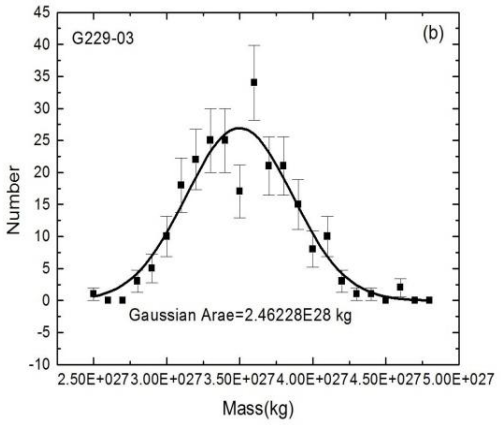

Figure 3: Gaussian Plot of Mass

The error bars where n represents several data in that bin. The value of dust mass in the cavity of interest was determined by following Hildebrand using a 100 μm IRAS image (Hildebrand, 1983). The dust mass in our region of interest was calculated by using distance to cavity (1300 pc) and flux densities of 343 pixels. The total mass of the cavity was found to be 8.50031 × 1029 kg which is higher than the study of Jha and Aryal in 2017 in which they found a total mass of structure was 2.55 × 1027 kg. The difference in the result can be related to the size of the cavity (Jha et al., 2017). The distribution of dust color temperature (Td) of the G229-03 Far infrared loop is represented in Figure 4 in which the solid curve represents the Gaussian fits.

A very good agreement between the observed and fitted curves was seen. In this study, large numbers of data were taken from our structure by making different contour levels, and to know the distribution of these data Gaussian distribution was used.

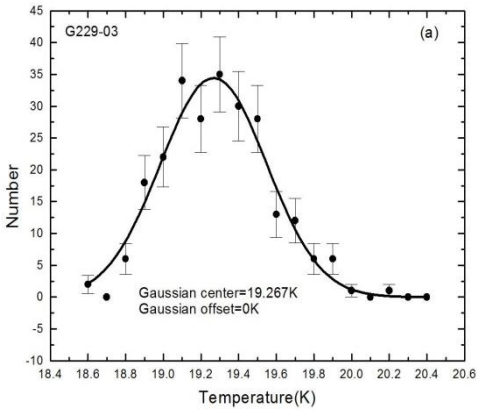

Figure 4: Gaussian Plot of Temperature

The minimum and maximum values of dust color temperature were found to be 18.63 ± 1.16 K and 20.24 ± 1.96 K respectively whereas the same dust color temperature varies from 19.4 ± 1.2 K and 25.3 ± 1.7 K according to Jha and Aryal in 2017 (Jha et al., 2017). The distribution of dust color temperature was found to be fitted nicely with Gaussian distribution with a Gaussian center of 19.26 K and with an offset of zero. The offset temperature of 0 K shows that data fits exactly with the Gaussian distribution as expected.

In figure-5, the plot shows flux density distribution between 100 μm and 60 μm. Here the scattered data increased with the value of relative flux density. The solid line in figure 5 shows the best fit line with a regression coefficient of 0.16774 and a standard deviation of 0.13877.

The regression coefficient is used to find the relationship between two or more variables. If the value of the regression coefficient was closer to the one then there will be a uniform distribution of flux along the mean or all points are approaching the mean. Here the regression coefficient of 0.1677 shows F(60μm) by 0.16774. The standard deviation shows how data points are spread around the mean. Here the value of standard deviation 0.13877 shows that it is widely spread around the mean, that for a unit change in the value of F(100μm) along the positive X-axis there was a rise in the value of the lower value of flux densities was found in the limited portion of the field, whereas the data were found to be

highly populated in most of the portions of the plot, especially in the middle portion. Overall, a good correlation between a distribution and fitted curve was observed.

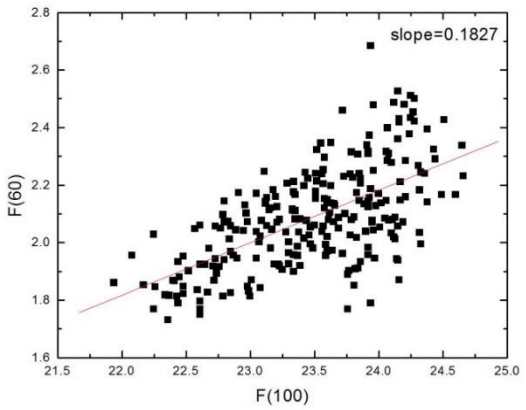

Figure 5: Scattered plot of flux at 60 μm and 100 μm

The inclination angle of the core or loop was greater than 60° which shows that the core region of our cavity was edge-on appearance. The inclination angle for the larger structure was found to be 13.71° which shows that the outer region is nearly face-on.

In this study, the loop was oriented by 45° to the plane of the sky. The value of inclination angle of the core region of the loop was found to be edge-on (i>60) whereas the larger structure was nearly face-on (i<60). The result complied with the results of Jha and Aryal, 2017(Jha et al., 2017). Figure 6 and figure 7 show the distribution of Planck's function along the major and minor diameters of the cavity.

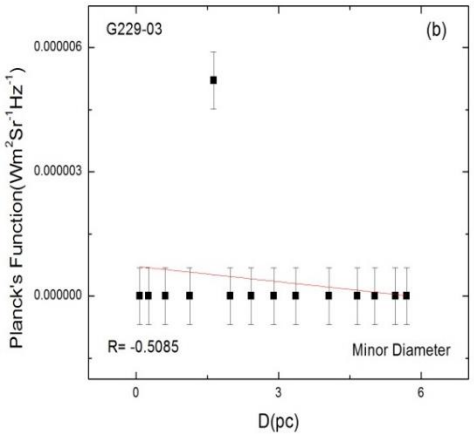

Figure 6: Variation of Planck's function (B) with the distance along a minor diameter

There was the almost same value of Planck's function with an increasing value of distance along the X-axis meaning that the value of Planck's function along the major and minor diameter was independent of distance. The result was in contradiction to the recent studies done by and Gautam and Chhatkuli, 2020 (Gautam & Chhatkuli, 2020) and Joshi et al., 2021 (Joshi et al., 2021).

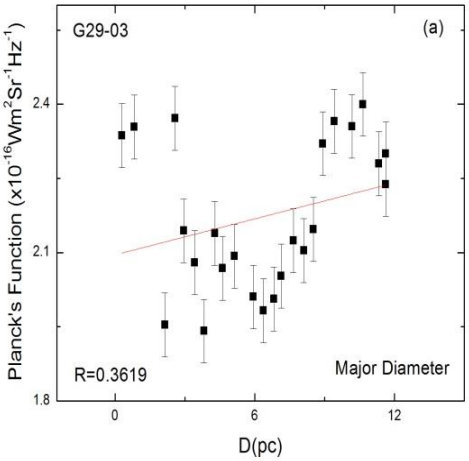

Figure 7: Variation of Planck's function (B) with the distance along major diameter

4. Conclusion

In this study, dust mass, dust color temperature, the inclination of the core region, and their distribution and compared with its larger or outer structure was studied to know whether the interested cavity was thermally (dynamical) stable or not. The Far-infrared loops were found to be located within a 1° radius around the high-velocity cloud. The inclination angle of the core or loop was greater than 60° which shows that the core region of the cavity of interest was edge-on appearance. The inclination angle for the larger structure was found to be 13.71° which shows that the outer region was nearly face-on. Additionally, the loop was oriented by 45° to the plane of the sky. The Gaussian distribution of temperature was well fitted with the center of 19.267 K which shows that the cavity was in thermal equilibrium and the outer region showed the offset temperature of about 35 K suggesting that the loop was dynamically unstable. The large-scale temperature was relatively higher than the temperature of the core region. The total mass of the loop was 8.50031×10^{29} kg which is about 0.425 times the mass of the Sun at a distance of 1300 pc. An offset temperature of less than 2 K shows that the core region of the cavity is relatively stable. The minimum and maximum temperatures were between 20.24 ±

1.16 K and 18.63 ± 1.96 K respectively. In the core region, the average temperature was 19.53 K, approximately equal to Gaussian center 19.267 K with an offset temperature of 0.4 K showing that the cavity is dynamically stable.

Acknowledgments

We are thankful to the SIMBAD database, Sky views virtual Observatory, ATNF pulsar catalog, IRAS surveys, and GIRL catalog. We are indebted to Prof. Ronald Weinberger of Innsbruck University, Innsbruck, Austria, for providing substantial data. We acknowledge University Grant Commission, Nepal for providing Master Research Support Grant.

Conflicts of Interest

The authors declare that there is no conflict of interest.

Funding

There is no funding resource.

References

Aryal, B., Rajbahak, C., & Weinberger, R. (2009). Planetary nebulae NGC 6826 and NGC 2899: early aspherical mass loss? Astrophysics and Space Science, 323(4), 323-327.

Aryal, B., Rajbahak, C., & Weinberger, R. (2010). A giant dusty bipolar structure around the planetary nebula NGC 1514. Monthly Notices of the Royal Astronomical Society, 402(2), 1307-1312.

Brand, P., & Zealey, W. (1975). Cloud structure in the galactic plane-A cosmic bubble bath. Astronomy and Astrophysics, 38, 363-371.

Dupac, X., Bernard, J.-P., Boudet, N., Giard, M., Lamarre, J.-M., Mény, C., . . . Stepnik, B. (2003). Inverse temperature dependence of the dust submillimeter spectral index. Astronomy & Astrophysics, 404(1), L11-L15.

Gautam, A., & Aryal, B. (2019). Study of far infrared cavity around a post AGB star under IRAS survey at galactic latitude-3°. BIBECHANA, 16, 23-30.

Gautam, A., & Chhatkuli, D. (2020). Planck Function Distribution in the Far Infrared Cavity nearby AGB Star at Galactic Latitude 0.6 º. Journal of Nepal Physical Society, 6(2), 97-103.

Hildebrand, R. H. (1983). The determination of cloud masses and dust characteristics from submillimetre thermal emission. Quarterly Journal of the Royal Astronomical Society, 24, 267.

Jha, A., & Aryal, B. (2018). Dust color temperature distribution of two FIR cavities at IRIS and AKARI maps. Journal of Astrophysics and Astronomy, 39(2), 1-7.

Jha, A., Aryal, B., & Weinberger, R. (2017). A study of dust color temperature and dust mass distributions of four far infrared loops. Revista mexicana de astronomía y astrofísica, 53(2).

Joshi, I. N., Jha, A. K., & Aryal, B. (2021). A study of dust structure nearby white dwarf WD1334-678. BIBECHANA, 18(2), 130-137.

Kiss, C., Moór, A., & Tóth, L. (2004). Far-infrared loops in the 2nd Galactic Quadrant. Astronomy & Astrophysics, 418(1), 131-141.

Könyves, V., Kiss, C., Moór, A., Kiss, Z., & Tóth, L. (2007). Catalogue of far-infrared loops in the Galaxy. Astronomy & Astrophysics, 463(3), 1227-1234.

Schulz, B., & Consortium, S. (2010). Observing Cold Dust with Herschel/SPIRE. AIP Conference Proceedings,

Wada, K., Spaans, M., & Kim, S. (2000). Formation of cavities, filaments, and clumps by the nonlinear development of thermal and gravitational instabilities in the interstellar medium under stellar feedback. The Astrophysical Journal, 540(2), 797.

Weinberger, R., & Armsdorfer, B. (2004). A Pair of 9° Long Dust Jets Ejected From Evolved Stars. Asymmetrical Planetary Nebulae III: Winds, Structure and the Thunderbird,